PAPER

Check for updates

Contaminant removal by efficient separation of *in situ* formed layered double hydroxide compounds from mine wastewaters†

Zoltán Somosi,[ab] Szabolcs Muráth, [iD][ab] Péter Nagy,[a] Dániel Sebők,[c] Istvan Szilagyi [iD] *[ab] and Grant Douglas*[d]

The efficient removal of a range of anionic and cationic contaminants from acid mine waters to facilitate water reuse or for safe discharge constitutes a major environmental challenge. Recently, layered double hydroxide (LDH)-type materials have shown considerable efficacy at experimental and full-scale for acid mine water treatment. In this study, LDH-type materials were prepared *in situ* under different experimental conditions with a method for their separation also developed. This work demonstrated that an interlinked network of smaller LDH aggregates was formed during synthesis leading to the development of stable colloids. Different approaches were tested to separate the solid materials containing the captured contaminants from the solute. Polyelectrolytes adsorbed strongly on the particle networks causing charge neutralization and overcharging, however, destabilization of the stable dispersions was unsuccessful. Diluting the stable dispersions led to rapid sedimentation and separation of the LDH, which facilitated higher solute recoveries.

Water impact

Numerous studies document LDH as an adsorbent for different contaminants present in wastewaters, but few consider the removal efficiency of the spent adsorbent. This study gives an insight into *in situ* formation of LDH in both model and in acidic mine water systems enhancing the understanding of adsorption, sedimentation and colloidal properties during the removal process.

1. Introduction

Over the past two decades in particular, the unique physico-chemical properties of layered double hydroxides (LDHs), often known more generically as hydrotalcites, have gained considerable attention in the research community,[1–4] and industry due to their application as sorbents or catalysts,[5–12] and for the treatment of mining or other wastewaters.[13–16] The utility of LDHs stems from their tuneable functional properties that may result from the substitution of a variety of cations into the metal double hydroxide layers and anions into the interlayer spaces. Anion and edge exchange, and the

[a] *MTA-SZTE Lendület Biocolloids Research Group, University of Szeged, H-6720 Szeged, Hungary. E-mail: szistvan@chem.u-szeged.hu*
[b] *Interdisciplinary Excellence Center, Department of Physical Chemistry and Materials Science, University of Szeged, H-6720 Szeged, Hungary*
[c] *Interdisciplinary Excellence Center, Department of Applied and Environmental Chemistry, University of Szeged, H-6720 Szeged, Hungary*
[d] *Centre for Environment and Life Sciences, CSIRO Land and Water, WA6913 Wembley, Australia. E-mail: grant.douglas@csiro.au*
† Electronic supplementary information (ESI) available. See DOI: 10.1039/c9ew00808j

presence of exchangeable surface hydroxyl groups collectively add to the range of possible applications.[3,17,18]

Layered double hydroxides have the general formula of $(M^{II}_{(1-x)}M^{III}_{(x)}(OH)_2)A^{n-}_{(n/2)} \cdot H_2O$, with $0.20 \leq x \leq 0.33$ and A^{n-} as the prevailing anion, thus yielding a range of primary M^{II} to M^{III} ratios of often mixed metal composition between 2:1 to 4:1. In the specific case of hydrotalcite, *sensu stricto*, M^{II} is Mg^{2+}, M^{III} is Al^{3+}, in a 2:1 to 3:1 molar ratio, and A^{n-} is CO_3^{2-}.[19] Notably, however, a variety of other alkaline earths, transition metals, rare earth elements, and some actinides[20] in addition to single anionic moieties, mixtures of anions, (metallo)oxyanions and on occasion, complex oxyanions[21] may be incorporated into the hydrotalcite structure to yield a mixed composition LDH. Compared to other nanoparticles used for removal of ionic contaminant,[22,23] one of the main advantages of the LDHs is the simultaneous capture of cations in the metal hydroxide layers and anions that are intercalated into the lamellar structure.

When utilized in industrial or mine water treatment for the removal of contaminants,[15,16,24] one of the major impediments in maximizing the recovery of treated water is the efficient separation of LDH, as small particles or

This journal is © The Royal Society of Chemistry 2019

Environ. Sci.: Water Res. Technol., 2019, **5**, 2251–2259 | 2251

View Article Online

aggregates may be present due to the short reaction times following addition of reagents and which form stable dispersions. Efficient removal of LDH would facilitate higher water recoveries for reuse or environmental discharge as well as to allow the reuse of a clarified effluent suitable for other treatment processes such as the removal of remaining nitrate or sulfate as commonly found in industrial and mine wastewaters *via* the application of microbial bioreactors.[25] Ion exchange and subsequent separation of other inorganic nanoparticles were carried out by polymer-induced aggregation,[26] nevertheless, no efficient removals of LDH used for decontamination of wastewater have been reported in the literature.

In this study, we have examined the colloidal stability of four types of LDH including two formed from the treatment of an acid mine water and two model hydrotalcite compositions using different Mg precursors, $Mg(OH)_2$ and $MgCl_2$ to (i) better elucidate the fundamental colloidal properties of these various types of LDH, and (ii) to investigate methods to induce colloidal instability to facilitate flocculation.

2. Materials and methods

2.1. Chemicals

The inorganic compounds ($MgCl_2 \cdot 6H_2O$, $NaAlO_2$, $NaOH$ and $Na_3PO_4 \cdot 12H_2O$, all purchased from VWR) were of analytical grade. A sodium salt of poly(styrene sulfonate) (PSS) (mol wt 10 kg mol^{-1}) was purchased from Sigma Aldrich and sodium salt of dextran sulfate (DXS) (mol wt 8 kg mol^{-1}) was purchased from Alfa Aesar. The polyelectrolyte and phosphate stock solutions were made by dissolving the solid materials in water and adjusting the pH to the desired value.

2.2. Dispersion synthesis

Four different samples were synthesized by a coprecipitation method. Sample 1 was prepared in demineralized water with the addition of $Mg(OH)_2$ and $NaAlO_2$ dissolved in NaOH to a final pH of 9.7 to form a 3 : 1 Mg : Al mol ratio hydrotalcite. Sample 2 was prepared in mine wastewater received from an acid (pH 4.5) mine water. Its major and trace element composition is shown in Table S1.† During the *in situ* LDH synthesis, the $NaAlO_2$ dissolved in NaOH was added to the wastewater sample to a final pH of 10, which decreased to a pH of *ca.* 8.5 in the atmosphere due to carbon dioxide absorption. Sample 3 was also prepared from an acid mine water. The $NaAlO_2$ dissolved in NaOH was added to the wastewater sample together with $Mg(OH)_2$ as a LDH substrate for nucleation to a final pH of 10. Sample 4 was prepared by the dissolution of $MgCl_2 \cdot 6H_2O$ in demineralized water followed by the addition of $NaAlO_2$ dissolved in NaOH under continuous stirring. Thereafter, 1 M NaOH was added dropwise to a final pH of 9.8 to form a 3 : 1 Mg : Al mol ratio hydrotalcite. The dispersion was then aged at 80 °C for two days to facilitate higher crystallinity, centrifuged and washed with demineralized water. All of the obtained materials were

stored in 10 g L^{-1} stock dispersions. In the experiments, they were diluted with electrolyte solutions of the same ionic strength and pH as in the original samples.

2.3. Solid analysis

To obtain solid samples for characterization, a part of the original LDH/hydrotalcite dispersions were separated *via* centrifugation (10 000 rpm, 5-times, 10 minutes each), washed with demineralised water and dried at 80 °C to avoid the loss of interlamellar water.

2.4. Characterization techniques

The LDH or hydrotalcite mineralogy was analysed by X-ray diffraction (XRD) with a PW 1830 diffractometer (Philips) using Cu-Kα radiation (λ = 0.1542 nm) and operated in Bragg–Brentano geometry with Ni filter at a voltage of 40 kV and a current of 30 mA. The diffractograms were recorded in the 4–80° 2-theta range with a step size of 0.02°. The powder samples were placed on a glass zero background holder for the acquisition of the XRD patterns.

Further investigation of the LDH or hydrotalcite structures was obtained from Fourier-transform infrared (FT-IR) spectra of the samples, which were recorded on a JASCO FTIR-4700 spectrometer equipped with a DTGS detector in attenuated total reflectance mode. Spectral resolution was 4 cm^{-1} with 256 scans collected for each spectrum. The spectra were recorded in the wavenumber range of 4000–600 cm^{-1}. The spectra were baseline-corrected and smoothed.

Electrophoretic mobility was measured with a LiteSizer 500 (Anton Paar) device equipped with a 40 mW laser source operating at 658 nm wavelength. Disposable plastic omega-shaped capillary cells (Anton Paar) were used for the measurements. During sample preparation, calculated amount of polyelectrolyte and phosphate stock solutions were mixed with appropriate amount of samples 1–4 to adjust the flocculants and particle concentrations. The pH of the dispersions used in the experiments was kept the same as in the original samples.

Dynamic light scattering (DLS) technique was used to measure the hydrodynamic size of the dispersed particles. The measurements were carried out with the same LiteSizer device as above at 175° scattering angle in disposable plastic cuvettes (VWR). The cumulant method was used to fit the correlation functions, which were collected for 20 seconds to determine the hydrodynamic radius of the particles.

The morphology of the solids was characterized by a Hitachi S-4700 scanning electron microscope (SEM). The surface of the samples was covered with gold *via* physical vapour deposition before the measurements, which were conducted with 10 kV accelerating voltage.

Energy dispersive X-ray analyzer (EDX, Röntec QX2 system) was coupled to the microscope to provide the occurrence of elements in the samples. For these measurements, accelerating voltage was set to 20 kV and noble metal deposition was omitted.

2252 | *Environ. Sci.: Water Res. Technol.*, 2019, **5**, 2251–2259

This journal is © The Royal Society of Chemistry 2019

The turbidity of the dispersions was assessed by recording the UV-visible (UV-vis) spectra with a Genesys 10S spectrophotometer (Thermo Scientific). The wavelength range used was 190–1100 nm with 0.1 nm scaling.

3. Results and discussion

3.1. LDH/Hydrotalcite characterization

Mineralogical analysis of the four samples indicates the presence of brucite in sample 1 formed using $Mg(OH)_2$ and $NaAlO_2$/NaOH as the precursor materials (Fig. 1). However, small peaks at *ca.* 12, 21 and 33 degrees 2θ suggest the presence of a minor hydrotalcite phase. The absence of hydrotalcite as a major phase may reflect the inefficient utilisation of $Mg(OH)_2$ in a colloidal form, which may have only undergone only incipient dissolution and/or surface reaction to form a small reaction rind containing hydrotalcite at the high pH following the addition of $NaAlO_2$/NaOH. In contrast, in sample 4 at 2:1 Mg:Al mol ratio, quintinite[27] was formed indicating only partial utilisation of the Mg used in the planned 3:1 Mg:Al mol ratio synthesis. Characteristic LDH reflections[28] were detected in sample 2 with no other crystalline substances found. Sample 3 was composed of both brucite and LDH indicating only partial use of $Mg(OH)_2$ as a precursor material. The crystallinity of the LDH was poor in both samples 2 and 3 formed from the acid mine water reflecting the polymetallic composition of the metal hydroxide layers and the likely variable anion occupancy in

the interlayers as identified in FT-IR analysis discussed below.

Using FT-IR analysis, a range of peaks can be identified, which give insight into the interlayer anions present (Fig. 2). In samples 2 and 3, an intense band was found at around 1090 cm^{-1} corresponding to the region of sulfate symmetric stretching vibrations indicating the intercalation of sulfate ions within the LDH and/or adsorption on the outer surface. In samples 1, 2 and 3, a peak at 1365 cm^{-1} corresponds to carbonate asymmetric stretching, which is shifted towards higher wavenumbers in sample 4. A peak around 1635 cm^{-1} present in all samples corresponds to the scissor vibration of water located in the LDH interlayer. In all systems, a peak occurring at 3400 cm^{-1} corresponds to the valence vibration of O–H groups of water molecules or of surface M–O–H functionalities within the metal hydroxide layer of the LDH or brucite.

The above findings indicate that hydrotalcite preparation to form a predominant crystalline phase was least successful in sample 1 with the possibility of sulfate and carbonate present in an LDH/hydrotalcite surface layer, while brucite-LDH composite was found in sample 3. In sample 2 and sample 4, an LDH derivative and quintinite were formed, respectively. Samples containing hydrotalcite as the predominant phase were able to remove considerable sulfate from the acid mine wastewater, intercalated between the metal hydroxide layers and also potentially present on the outer surface. This has important implications, in particular
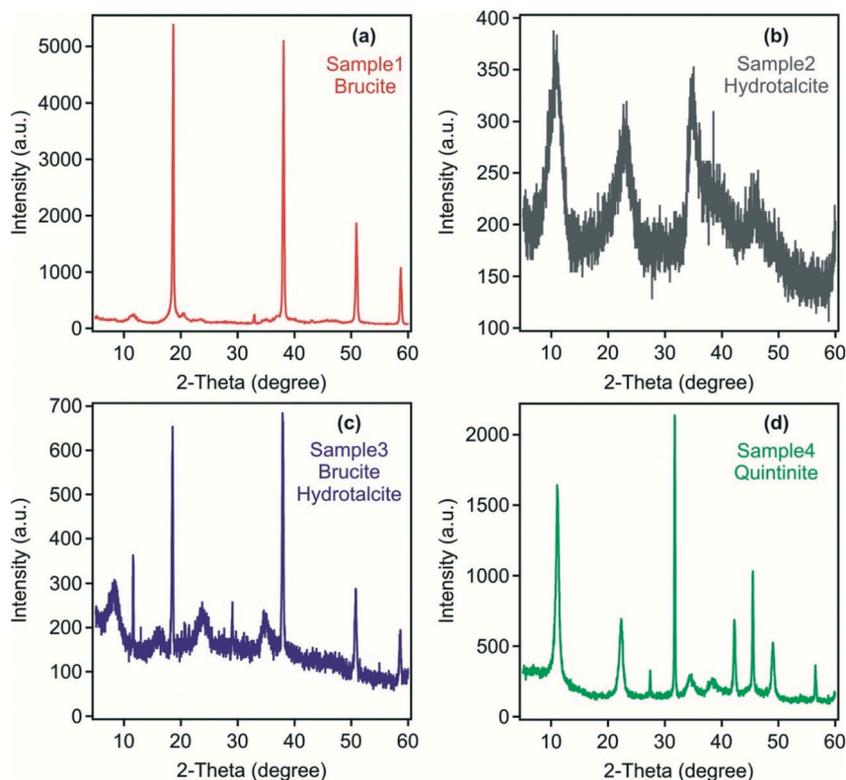

Fig. 1 Powder XRD patterns of the solid materials obtained from (a) sample 1, (b) sample 2, (c) sample 3 and (d) sample 4.

This journal is © The Royal Society of Chemistry 2019

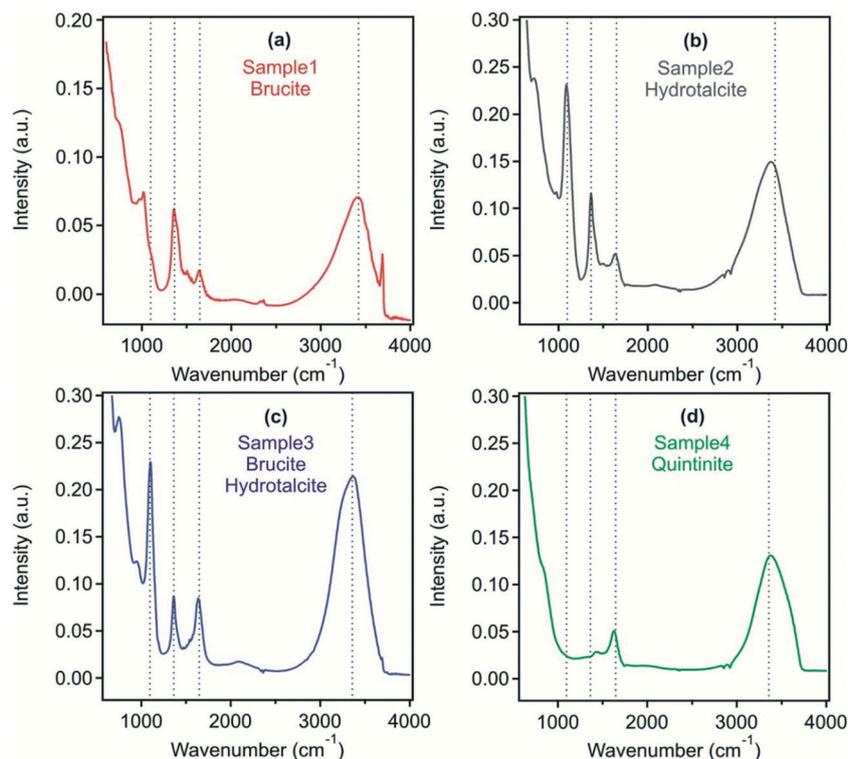*Environ. Sci.: Water Res. Technol.*, 2019, **5**, 2251–2259 | **2253**

Fig. 2 FT-IR spectra of (a) sample 1, (b) sample 2, (c) sample 3 and (d) sample 4.

to reduce sulfate level that is discharged to the environment, or as a reduced sulfate feedwater to sulfate-reducing bioreactors.

Electrophoretic mobilities of the samples were measured to assess the surface charge properties of the LDH and hydrotalcite particles, which were predominantly in the form of stable dispersions and as a starting point to investigate destabilisation pathways. The electrophoretic mobility for samples 1–4 were 8.9×10^{-9}, 5.8×10^{-9}, 4.3×10^{-9}, 4.8×10^{-9} m^2 Vs^{-1}, respectively (Fig. 3) indicating a small positive surface charge of the materials in the dispersions with the similarity of all measurements consistent with the formation of a LDH/hydrotalcite layer on the Mg(OH)$_2$ used as a precursor material in sample 1. This positive charge originates from the structure in the case of LDH/hydrotalcite[29] and quintinite,[30] while from the high isoelectric point and subsequent presence of protonated hydroxide groups for the brucite.[31,32] All measurements were carried out at an ionic strength of 80 mM corresponding to the ionic strength of the acidic mine water that was used for the experiments.

3.2. Particle destabilisation

Polyelectrolytes and multivalent ions have proven to be effective flocculation agents during water treatment[33,34] and also in dispersions containing hydrotalcite.[35,36] Surface charge properties and aggregation processes are often intimately related,[37–39] therefore, the effect of possible adsorption of negatively charged PSS, DXS and phosphate ions on the charging features was investigated at different flocculant concentrations.

Electrophoretic mobilities as a function of polyelectrolyte and phosphate concentrations are shown in Fig. 3. The mobilities of the brucite-containing systems (samples 1 and 3) were positive at low flocculant concentrations under the conditions investigated. In contrast, mobilities close to zero were measured in the LDH and hydrotalcite (quintinite) containing systems (samples 2 and 4) at low polyelectrolyte and phosphate concentrations. Such a reduced electrophoretic mobility is most likely due to the high ionic strength of *ca.* 80 mM in the dispersions, since elevated salt concentrations usually lead to screening of the surface charge and decreased mobility.[40] For samples 1 and 3, charge neutralization occurred due to the adsorption of the negatively charged PSS, DXS and phosphate ions. The concentrations corresponding to the charge neutralization points are shown in Table S2.† Similar charge neutralization processes often give rise to rapid particles aggregation and to destabilization of colloidal samples.[35,37,41–44]

With increasing flocculant dose, particle surface charge became negative due to the progressive adsorption of negatively charged species onto the LDH/hydrotalcite surface. Similar charge reversal effects have been reported previously in systems containing colloidal particles and multivalent ions or polyelectrolytes[45–47] and also for LDH.[35] This phenomenon originates from the entropy gain due to the release of solvent molecules and counterions upon adsorption, from the

2254 | *Environ. Sci.: Water Res. Technol.*, 2019, **5**, 2251–2259

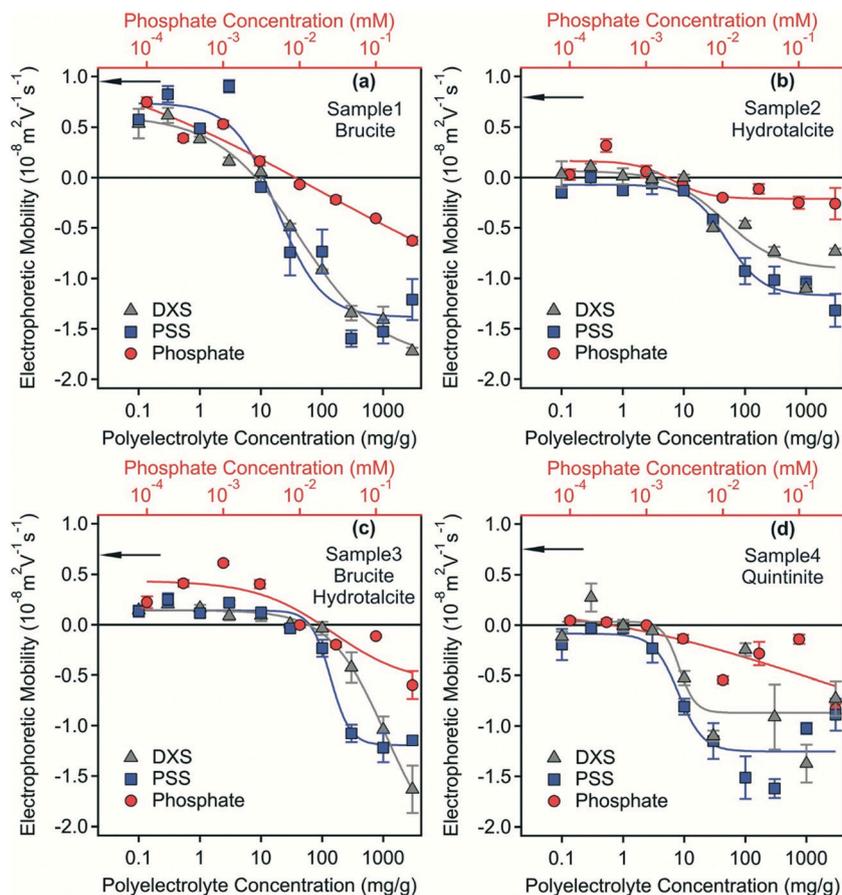This journal is © The Royal Society of Chemistry 2019

Fig. 3 Electrophoretic mobilities of particles dispersed in samples 1–4 ((a) sample 1, (b) sample 2, (c) sample 3 and (d) sample 4) as a function of the polyelectrolyte (PSS and DXS) and phosphate concentration. An ionic strength of 80 mM was kept constant in the experiments. The solid lines are for guidance. Arrows indicate the mobilities of the particles prior to flocculants addition.

laterally heterogeneous polyelectrolyte adsorption and from the attractive hydrophobic interaction between the polyelectrolyte and the surface.[37] Adsorption of PSS and DXS caused higher magnitude of charge reversal at high flocculant concentration than phosphate owing to their excess of unbound negative charge centres following surface adsorption. Previous studies[33,35,37,41,48] indicate that stable dispersions can also form at high flocculant doses, while destabilization of the dispersions are expected at the isoelectric points. In the four separate samples investigated here spanning model systems (samples 1 and 4) and real-world systems derived from acid mine waters (samples 2 and 3), effective destabilisation could not be achieved despite the use of two separate polyelectrolytes or phosphate. This phenomenon is investigated further below.

An investigation of the on-going stability of the dispersions was undertaken using DLS. Hydrodynamic radii ranged from 600 nm to 3000 nm in the samples with a polydispersity factor of approximately 0.8. While these data indicated that DLS was not a suitable technique to measure particle size and study aggregation behaviour in the samples, the DLS results suggest that the dispersions are probably composed of a network of aggregates or particles forming

colloidal gel-like structures, which usually occurs at high particle concentrations, where the dispersed materials interlink in a stable 3D framework occupied by interstitial water moleclues.[49–52] Such structures may be further stabilized by steric forces caused by the overlap of the adsorbed polyelectrolyte chains. The presence of these types of interactions has been reported in other polyelectrolyte-particle systems.[35,53]

To further investigate particle or aggregate morphology, SEM images were obtained (Fig. 4). It was found that the brucite and LDH or quintinite particles formed aggregated networks of few microns in diameter that may reflect their original hydrated structure. All samples tended to contain primary particles of a few hundred nanometers in diameter. Aggregate diameters were typically 1–3 μm. The SEM study revealed particles with irregular morphology, common to hydrotalcites and related materials synthesized by co-precipitation.[13,54] The mixed chemical composition of sample 3 was also apparent with distinctly different crystal/aggregate morphologies observable.

To explore the composition of the solid materials, EDX analysis was performed on the aggregated samples (Fig. S1 and S2†). In sample 1, Mg and Al are uniformly distributed,
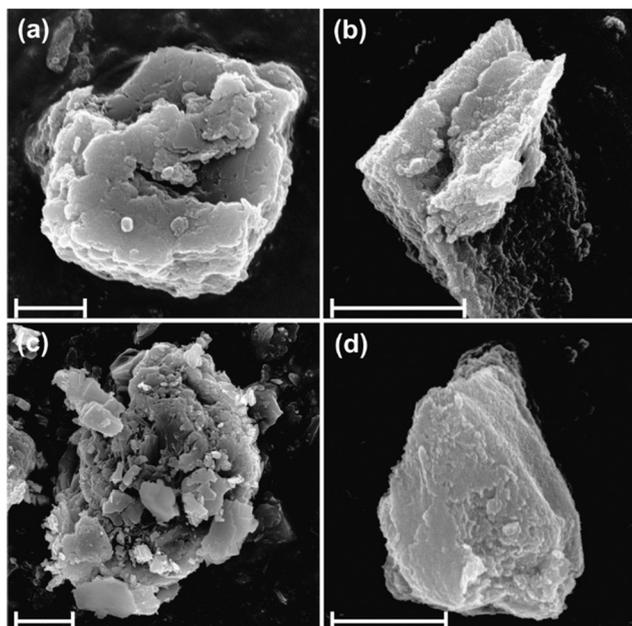
Fig. 4 SEM images of (a) sample 1, (b) sample 2, (c) sample 3 and (d) sample 4. The scale bars indicate 1 micrometer dimension.

however, according its XRD pattern, brucite is the main component and LDH is present only in small amounts, probably as a surface reaction rind. The elemental compositions of samples 2 and 3 are similar. These materials are intercalated with sulfate ions as confirmed in the EDX spectra and also in the FT-IR results discussed earlier. Regarding sample 4, while also containing the layer forming Mg and Al metals (like in samples 2 and 3), it has high chloride content consistent with the use of $MgCl_2$, as a precursor reagent.

Based on information from DLS, in which suggested the presence of complex aggregates, the absorbance of the samples was measured as a turbidity proxy. This approach was successfully applied to investigate aggregation and sedimentation processes in non-transparent and polydisperse samples similar to those in the present study.[48,55] As the UV-vis spectra indicated that none of the samples have a specific absorption around 450 nm, this wavelength was chosen to study the dispersion stability. Absorbance values recorded with the original samples during 60 minutes are shown in Fig. S3† and confirm that all samples formed stable dispersions.

As discussed above, neutralizing the charge of colloidal particles often leads to rapid aggregation and to unstable dispersions, from which the solids may settle.[35,37,41] This phenomenon may be particularly advantageous in environmental applications, where contaminant-laden LDH/hydrotalcite needs to be removed prior to wastewater reuse or environmental discharge.[13] With the development of a neutral charge, it is expected that repulsive interparticle interaction will be eliminated, thus leading to the destabilization of the particle aggregates.[40] Time-resolved absorbance data of the original dispersions in the presence of the flocculants discussed above, whose dose was set to the

isoelectric points (Table S2†), were recorded, however, little change in settling rates irrespective of the addition of either the PSS or DXS polyelectrolytes or phosphate was observed apart from the quintinite system in sample 4 (Fig. S4†).

Since the net charge of the particles was adjusted to close to zero via polyelectrolyte or phosphate addition, it can be assumed that the interaction between the aggregates and the stabilizing force between the colloidal networks is of non-electrostatic origin. Most likely, hydrophobic forces, steric and secondary chemical interactions such as hydrogen bonds are responsible for the interlinking between the particles and subsequent evolution of the stable 3D structures.

Since the formation of such interlinked materials occurs usually at high solid concentrations,[50] the effect of dilution on the stability of the samples was investigated by measuring the time-resolved absorbance. Accordingly, samples 1 to 4 were diluted 10-fold with water, in which the pH and ionic strength were adjusted as per the original samples and time-resolved absorbance values were recorded over 60 minutes (Fig. 5).

For sample 1, rapid sedimentation was observed within five minutes indicating the destruction of the gel-like 3D structure. Similar behaviour occurred in samples 2 and 3, where complete sedimentation occurred after 25 and 20 minutes, respectively. These findings confirm the presence of interlinked particles and aggregates in the raw systems, which usually evolve at high particle concentrations, but simple dilution leads to the breakdown of the 3D network. For samples 2 and 3, the absorbance increased for a short time interval (15 and 10 minutes, respectively). This is due to the in vitro sedimentation process, which results in a transiently higher solids concentration of settling samples in the laser path. The pH of the samples was measured before and after the destabilization experiments and found to be stable (i.e., the initial and final pH was the same within the experimental error) during the measurements.

In contrast to samples 1 to 3, the turbidity of sample 4 decreased only slightly after 10-fold dilution over 60 minutes. Thus, it appears that a pure quintinite system is inherently more stable than that or either brucite/LDH or a mixed composition LDH.

To further study the effect of dilution on sedimentation, similar time-resolved settling measurements were carried out at several dilution rates. Accordingly, samples 1–4 were diluted to between 1 in 5 and 1 in 20 times the original sample suspended solid concentration with the pH and the ionic strength maintained as per the original samples with the time needed for the 50% decrease in the maximum absorbance measured (Fig. 6).

Sedimentation was markedly different depending on the composition of the solids and the extent of dilution. No net sedimentation was observed in sample 4 despite the substantial dilution factor employed. For sample 1–3, there was an initially steep decrease in the sedimentation time with increasing dilution with the most rapid sedimentation observed for sample 1 in the range at 5- to 10-fold dilution
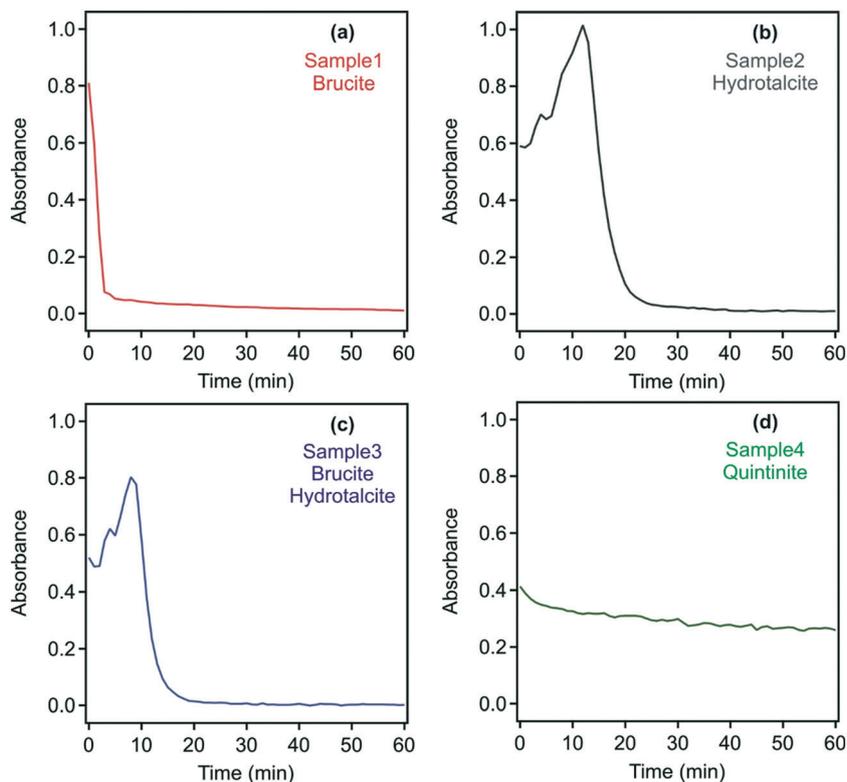
Fig. 5 Time-resolved absorbance measurements performed at 450 nm for samples 1–4 ((a) sample 1, (b) sample 2, (c) sample 3 and (d) sample 4). The original samples were 10x diluted with water (pH and ionic strength was adjusted as per the original samples), which results in a solid content of about 1000 mg L^{-1}.

with a minimum sedimentation time of 125 seconds. For sample 2, sedimentation rapidly increased between 10- and 15-fold dilution with a minimum sedimentation time of 235 seconds. For sample 3, sedimentation also rapidly increased between 10- and 15-fold dilution with a minimum sedimentation time of 370 seconds.

It is apparent from this study both the morphology and composition of the LDH/hydrotalcite influences the threshold to sedimentation as exemplified by the relative stability of quintinite aggregates. In more complex systems, however, dilution is a simple and effective method to induce 3D aggregate instability that will regulate the rate of and extent of recovery of contaminant-bearing LDH in wastewater or acid mine water treatment applications. Importantly, we have observed settling rates of >10 m per day for *ca.* 1 g L^{-1} polymetallic LDH formed *in situ* in an acidic mine pit water.[13] This high settling rate is similar to that achieved in this study after dilution to reduce total solids to similar (*ca.* 1 g L^{-1} or less) concentrations (Fig. 5 and 6). This is particularly pertinent where effective solid phase contaminant removal *via* settling is required prior to solute reuse or environmental discharge.
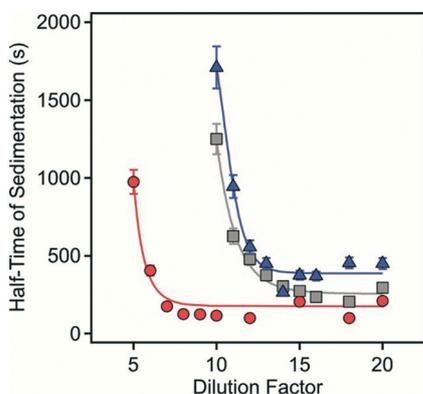
4. Conclusions

In situ formation of LDH compounds in model systems and acidic mine water was undertaken. The structures of the hydrotalcite compounds of different types were studied. Within the acid mine water hydrotalcites, considerable metal contaminant incorporation and sulfate adsorption occurred. Polyelectrolytes and multivalent ions failed to separate the adsorbent LDH materials from the samples due to the formation of highly stable colloidal gel-like structure. Following a reduction of the volume fraction of the solid content by dilution, an efficient separation procedure was developed including the breakdown of the gel-like structure and rapid sedimentation of the particles. The results of this study present a practical pathway to

Fig. 6 Half time of sedimentation as a function of the dilution factor for sample 1 (circles), sample 2 (squares) and sample 3 (triangles).

This journal is © The Royal Society of Chemistry 2019

Environ. Sci.: Water Res. Technol., 2019, **5**, 2251–2259 | 2257

facilitate the removal of *in situ* formed, contaminant-bearing LDHs from wastewaters.

Conflicts of interest

The authors declare no competing financial interest.

Acknowledgements

References

1 M. V. Bukhtiyarova, A review on effect of synthesis conditions on the formation of layered double hydroxides, *J. Solid State Chem.*, 2019, **269**, 494–506.

2 P. Lu, Y. Liu, T. T. Zhou, Q. Wang and Y. S. Li, Recent advances in layered double hydroxides (LDHs) as two-dimensional membrane materials for gas and liquid separations, *J. Membr. Sci.*, 2018, **567**, 89–103.

3 G. Mishra, B. Dash and S. Pandey, Layered double hydroxides: A brief review from fundamentals to application as evolving biomaterials, *Appl. Clay Sci.*, 2018, **153**, 172–186.

4 R. Trujillano, I. González-García, A. Morato and V. Rives, Controlling the synthesis conditions for tuning the properties of hydrotalcite-like materials at the nano scale, *ChemEngineering*, 2018, **2**, 31.

5 J. Cao, T. Y. Chen, B. S. Jin, Y. J. Huang and C. H. Hu, Structural efects of HCl adsorption on Mg-Fe hydrotalcite-like oxides at 350-650 degrees C in flue gas, *Ind. Eng. Chem. Res.*, 2018, **57**, 14939–14947.

6 F. Coumans, S. Mitchell, J. Schutz, J. Medlock and J. Perez-Ramirez, Hydrotalcite-derived mixed oxides for the synthesis of a key vitamin A intermediate reducing waste, *ACS Omega*, 2018, **3**, 15293–15301.

7 U. Sikander, S. Sufian and M. A. Salam, A review of hydrotalcite based catalysts for hydrogen production systems, *Int. J. Hydrogen Energy*, 2017, **42**, 19851–19868.

8 K. Swirk, M. Rønning, M. Motak, P. Beaunier, P. Da Costa and T. Grzybek, Ce- and Y-modified double-layered hydroxides as catalysts for dry reforming of methane: on the effect of Yttrium promotion, *Catalysts*, 2019, **9**, 56.

9 W. Y. Hernandez, J. Lauwaert, P. Van der Voort and A. Verberckmoes, Recent advances on the utilization of layered double hydroxides (LDHs) and related heterogeneous catalysts in a lignocellulosic-feedstock biorefinery scheme, *Green Chem.*, 2017, **19**, 5269–5302.

10 J. F. Yu, Q. Wang, D. O'Hare and L. Y. Sun, Preparation of two dimensional layered double hydroxide nanosheets and their applications, *Chem. Soc. Rev.*, 2017, **46**, 5950–5974.

11 K. H. Goh, T. T. Lim and Z. L. Dong, Enhanced arsenic removal by hydrothermally treated nanocrystalline Mg/Al layered double hydroxide with nitrate intercalation, *Environ. Sci. Technol.*, 2009, **43**, 2537–2543.

12 B. Ma, A. Fernandez-Martinez, S. Grangeon, C. Tournassat, N. Findling, S. Carrero, D. Tisserand, S. Bureau, E. Elkaim, C. Marini, G. Aquilanti, A. Koishi, N. C. M. Marty and L. Charlet, Selenite uptake by Ca-Al LDH: A description of intercalated anion coordination geometries, *Environ. Sci. Technol.*, 2018, **52**, 1624–1632.

13 G. B. Douglas, Contaminant removal from acidic mine pit water via in situ hydrotalcite formation, *Appl. Geochem.*, 2014, **51**, 15–22.

14 G. Douglas, M. Shackleton and P. Woods, Hydrotalcite formation facilitates effective contaminant and radionuclide removal from acidic uranium mine barren lixiviant, *Appl. Geochem.*, 2014, **42**, 27–37.

15 M. Zubair, M. Daud, G. McKay, F. Shehzad and M. A. Al-Harthi, Recent progress in layered double hydroxides (LDH)-containing hybrids as adsorbents for water remediation, *Appl. Clay Sci.*, 2017, **143**, 279–292.

16 J. M. Gong, T. Liu, X. Q. Wang, X. L. Hu and L. Z. Zhang, Efficient removal of heavy metal ions from aqueous systems with the assembly of anisotropic layered double hydroxide nanocrystals@carbon nanosphere, *Environ. Sci. Technol.*, 2011, **45**, 6181–6187.

17 C. Forano, F. Bruna, C. Mousty and V. Prevot, Interactions between biological cells and layered double hydroxides: Towards functional materials, *Chem. Rec.*, 2018, **18**, 1150–1166.

18 Z. Gu, J. J. Atherton and Z. P. Xu, Hierarchical layered double hydroxide nanocomposites: structure, synthesis and applications, *Chem. Commun.*, 2015, **51**, 3024–3036.

19 F. Cavani, F. Trifiro and A. Vaccari, Hydrtalcite-type anionic clays: Preparation, properties and applications, *Catal. Today*, 1991, **11**, 173–301.

20 M. Grafe, K. G. Bunney, S. Cumberland and G. Douglas, Mechanisms of uranyl sequestration by hydrotalcite, *ACS Omega*, 2017, **2**, 7112–7119.

21 S. Omwoma, W. Chen, R. Tsunashima and Y. F. Song, Recent advances on polyoxometalates intercalated layered double hydroxides: From synthetic approaches to functional material applications, *Coord. Chem. Rev.*, 2014, **258**, 58–71.

22 Y. X. Huang, A. N. Fulton and A. A. Keller, Optimization of porous structure of superparamagnetic nanoparticle adsorbents for higher and faster removal of emerging organic contaminants and PAHs, *Environ. Sci.: Water Res. Technol.*, 2016, **2**, 521–528.

23 K. Simeonidis, S. Mourdikoudis, E. Kaprara, M. Mitrakas and L. Polavarapu, Inorganic engineered nanoparticles in drinking water treatment: a critical review, *Environ. Sci.: Water Res. Technol.*, 2016, **2**, 43–70.

24 N. Chubar, R. Gilmour, V. Gerda, M. Micusik, M. Omastova, K. Heister, P. Man, J. Fraissard and V. Zaitsev, Layered double hydroxides as the next generation inorganic anion exchangers: Synthetic methods versus applicability, *Adv. Colloid Interface Sci.*, 2017, **245**, 62–80.

2258 | *Environ. Sci.: Water Res. Technol.*, 2019, **5**, 2251–2259

This journal is © The Royal Society of Chemistry 2019

25 K. Y. Cheng, A. H. Kaksonen and G. B. Douglas, Sequential in situ hydrotalcite precipitation and biological denitrification for the treatment of high-nitrate industrial effluent, *Bioresour. Technol.*, 2014, **172**, 373–381.

26 N. L. Torad, A. Takahashi, M. Kawakami, T. Kawamoto and H. Tanaka, Decontamination of very dilute Cs in seawater by a coagulation-precipitation method using a nanoparticle slurry of copper hexacyanoferrate, *Environ. Sci.: Water Res. Technol.*, 2019, **5**, 1328–1338.

27 E. S. Zhitova, V. N. Yakovenchuk, S. V. Krivovichev, A. A. Zolotarev, Y. A. Pakhomovsky and G. Y. Ivanyuk, Crystal chemistry of natural layered double hydroxides. 3. The crystal structure of Mg,Al-disordered quintinite-2H, *Mineral. Mag.*, 2010, **74**, 841–848.

28 D. G. Evans and R. C. T. Slade, in *Layered Double Hydroxides*, ed. X. Duan and D. G. Evans, 2006, vol. 119, pp. 1–87.

29 Z. P. Xu, Y. G. Jin, S. M. Liu, Z. P. Hao and G. Q. Lu, Surface charging of layered double hydroxides during dynamic interactions of anions at the interfaces, *J. Colloid Interface Sci.*, 2008, **326**, 522–529.

30 J. H. Kim, J. A. Park, J. K. Kang, J. W. Son, I. G. Yi and S. B. Kim, Characterization of quintinite particles in fluoride removal from aqueous solutions, *Environ. Eng. Res.*, 2014, **19**, 247–253.

31 H. Schott, Eelectrokinetic studies of magnesium-hydroxide, *J. Pharm. Sci.*, 1981, **70**, 486–489.

32 G. A. Parks, The isoelectric points of solid oxides, solid hydroxides, and aqueous hydroxo complex systems, *Chem. Rev.*, 1965, **65**, 177–198.

33 B. Bolto and J. Gregory, Organic polyelectrolytes in water treatment, *Water Res.*, 2007, **41**, 2301–2324.

34 R. J. Honda, V. Keene, L. Daniels and S. L. Walker, Removal of TiO$_2$ nanoparticles during primary water treatment: Role of coagulant type, dose, and nanoparticle concentration, *Environ. Eng. Sci.*, 2014, **31**, 127–134.

35 M. Pavlovic, P. Rouster, T. Oncsik and I. Szilagyi, Tuning colloidal stability of layered double hydroxides: from monovalent ions to polyelectrolytes, *ChemPlusChem*, 2017, **82**, 121–131.

36 C. Vasti, A. Borgiallo, C. E. Giacomelli and R. Rojas, Layered double hydroxide nanoparticles customization by polyelectrolyte adsorption: mechanism and effect on particle aggregation, *Colloids Surf., A*, 2017, **533**, 316–322.

37 I. Szilagyi, G. Trefalt, A. Tiraferri, P. Maroni and M. Borkovec, Polyelectrolyte adsorption, interparticle forces, and colloidal aggregation, *Soft Matter*, 2014, **10**, 2479–2502.

38 M. Borkovec, I. Szilagyi, I. Popa, M. Finessi, P. Sinha, P. Maroni and G. Papastavrou, Investigating forces between charged particles in the presence of oppositely charged polyelectrolytes with the multi-particle colloidal probe technique, *Adv. Colloid Interface Sci.*, 2012, **179**, 85–98.

39 M. Borkovec and G. Papastavrou, Interactions between solid surfaces with adsorbed polyelectrolytes of opposite charge, *Curr. Opin. Colloid Interface Sci.*, 2008, **13**, 429–437.

40 D. F. Evans and H. Wennerstrom, *The colloidal domain*, John Wiley, New York, 1999.

41 S. Muráth, S. Sáringer, Z. Somosi and I. Szilagyi, Effect of ionic compounds of different valences on the stability of titanium oxide colloids, *Colloids Interfaces*, 2018, **2**, 32.

42 K. L. Chen, S. E. Mylon and M. Elimelech, Enhanced aggregation of alginate-coated iron oxide (hematite) nanoparticles in the presence of, calcium, strontium and barium cations, *Langmuir*, 2007, **23**, 5920–5928.

43 I. Popa, G. Gillies, G. Papastavrou and M. Borkovec, Attractive and repulsive electrostatic forces between positively charged latex particles in the presence of anionic linear polyelectrolytes, *J. Phys. Chem. B*, 2010, **114**, 3170–3177.

44 A. Zaccone, H. Wu, M. Lattuada and M. Morbidelli, Correlation between colloidal stability and surfactant adsorption/association phenomena studied by light scattering, *J. Phys. Chem. B*, 2008, **112**, 1976–1986.

45 J. Lyklema, Overcharging, charge reversal: Chemistry or physics?, *Colloids Surf., A*, 2006, **291**, 3–12.

46 S. Ravindran and J. Wu, Overcharging of nanoparticles in electrolyte solutions, *Langmuir*, 2004, **20**, 7333–7338.

47 M. Quesada-Perez, E. Gonzalez-Tovar, A. Martin-Molina, M. Lozada-Cassou and R. Hidalgo-Alvarez, Overcharging in colloids: Beyond the Poisson-Boltzmann approach, *ChemPhysChem*, 2003, **4**, 235–248.

48 M. Kobayashi, S. Yuki and Y. Adachi, Effect of anionic surfactants on the stability ratio and electrophoretic mobility of colloidal hematite particles, *Colloids Surf., A*, 2016, **510**, 190–197.

49 P. Sandkuhler, J. Sefcik and M. Morbidelli, Kinetics of aggregation and gel formation in concentrated polystyrene colloids, *J. Phys. Chem. B*, 2004, **108**, 20105–20121.

50 T. Gisler, R. C. Ball and D. A. Weitz, Strain hardening of fractal colloidal gels, *Phys. Rev. Lett.*, 1999, **82**, 1064–1067.

51 M. Elimelech, J. Gregory, X. Jia and R. A. Williams, *Particle deposition and aggregation: Measurement, modeling, and simulation*, Butterworth-Heinemann Ltd., Oxford, 1995.

52 M. Tomsic, F. Prossnigg and O. Glatter, A thermoreversible double gel: Characterization of a methylcellulose and kappa-carrageenan mixed system in water by SAXS, DSC and rheology, *J. Colloid Interface Sci.*, 2008, **322**, 41–50.

53 T. Phenrat, N. Saleh, K. Sirk, H. J. Kim, R. D. Tilton and G. V. Lowry, Stabilization of aqueous nanoscale zerovalent iron dispersions by anionic polyelectrolytes: Adsorbed anionic polyelectrolyte layer properties and their effect on aggregation and sedimentation, *J. Nanopart. Res.*, 2008, **10**, 795–814.

54 J. S. Wu, Y. K. Xiao, J. Y. Wan and L. R. Wen, The growth mechanism of hydrotalcite crystal, *Sci. China Technol. Sci.*, 2012, **55**, 872–878.

55 S. H. Xu and Z. W. Sun, Progress in coagulation rate measurements of colloidal dispersions, *Soft Matter*, 2011, **7**, 11298–11308.

This journal is © The Royal Society of Chemistry 2019

Environ. Sci.: Water Res. Technol., 2019, **5**, 2251–2259 | **2259**